Evidence for a spin-correlated crystal field - two-photon spectroscopy of thulium III in the elpasolite $Cs_2NaYCl_6$:Tm



2001 J. Phys.: Condens. Matter 13 7403

(http://iopscience.iop.org/0953-8984/13/33/320)

INSTITUTE OF PHYSICS PUBLISHING JOURNAL OF PHYSICS: CONDENSED MATTER

J. Phys.: Condens. Matter **13** (2001) 7403–7419 PII: S0953-8984(01)25024-3

# Evidence for a spin-correlated crystal field—two-photon spectroscopy of thulium III in the elpasolite $Cs_2NaYCl_6$:Tm

**J R G Thorne, Qinghua Zeng and R G Denning**[1]

Department of Chemistry, University of Oxford, Inorganic Chemistry, South Parks Road, Oxford OX1 3QR, UK

Received 18 May 2001, in final form 27 June 2001
Published 2 August 2001
Online at stacks.iop.org/JPhysCM/13/7403

**Abstract**

We present two-photon excitation spectra for thulium III in the elpasolite $Cs_2NaYCl_6$:Tm. 37 out of the total of 40 crystal-field (CF) levels have been assigned, with the aid of a one-electron CF Hamiltonian, representing the most extensive data set so far reported for Tm III at a cubic site. Deviations from the predictions of the one-electron CF model are unusually large, the effective fourth-rank CF parameter being 60% larger for the singlet states than for the triplet states. This is discussed in terms of a spin-polarized covalency that is more pronounced in the singlet states of the metal ion.

## 1. Introduction

Two-photon fluorescence excitation (TPE) spectroscopy, using a tuneable nanosecond pulsed laser, provides a good probe of parity-conserving transitions in the solid state that are inaccessible to one-photon spectroscopy. We have used this technique previously to obtain polarized f–f spectra of Tb III, Eu III and Sm III ions [1–4] free of phonon structure, which conclusively identify large numbers of crystal-field (CF) levels. Although some 100 or so electronic states can be identified in each of these ions, these constitute a small fraction of the full manifold of the $f^N$-states. As such, they provide only limited scope for testing an empirical Hamiltonian. We now report the energies of almost all the 40 f-electron states expected for the much simpler case of the $f^{12}$ Tm III ion at a cubic site, with the aim of identifying more clearly the limitations of a conventional Hamiltonian.

A lanthanide ion can usually be adequately described by a free-ion Hamiltonian, together with a CF potential that acts to perturb the free-ion states. The former contains contributions from Coulombic ($F^k$, $k = 2, 4, 6$), electrostatically correlated Coulombic ($\alpha$, $\beta$, $\gamma$), spin–orbit coupling ($\zeta_{so}$), two electron spin-other-orbit ($M^k$, $k = 0, 2, 4$) and electrostatically correlated spin–orbit ($P^k$, $k = 2, 4, 6$) interactions.

[1] Author to whom correspondence should be addressed.

  

The CF is expressed as the sum of one-electron operators:

$$H_{CF} = \sum_{i,k,q} B_q^{(k)} u_q^{(k)}(i) \tag{1}$$

where $u_q^{(k)}(i)$ is a unit tensor operator for the $i$th f-electron, of rank $k$ where $k = 2, 4, 6$ and $q$ is restricted by symmetry. A rigorous test of the validity of this simple model needs a large energy level data set, and a small number of CF parameters. The cubic environment provided by the elpasolite lattice requires only two such parameters and is ideal for this purpose.

A more realistic Hamiltonian introduces the influence of electron-correlation on the CF [5, 6], and includes a spin-correlated part, the spin-correlated crystal field (SCCF) described by the additional perturbation:

$$H_{SCCF} = \sum_{i,k,q} b_q^{(k)} \boldsymbol{S} \cdot \boldsymbol{s}_i u_q^{(k)}(i). \tag{2}$$

The parameters $b_q^{(k)}$ are a measure of the modification to the CF arising from the dependence of the radial part of the wavefunction of the $i$th 4f-electron on its spin orientation $\boldsymbol{s}_i$ relative to the total spin $\boldsymbol{S}$, in response to exchange interactions. The relative importance of these SCCF corrections is measured by the parameters $c_q^{(k)} = b_q^{(k)}/B_q^{(k)}$ such that

$$H_{TOTAL} = H_{CF} + H_{SCCF} = \sum_{i,k,q} B_q^{(k)} u_q^{(k)}(i)\{1 + \boldsymbol{S} \cdot \boldsymbol{s}_i c_q^{(k)}\}. \tag{3}$$

However, alternative physical mechanisms can also be described by this form of parametrization. One such is an increase in the CF attributable to a general radial expansion in any higher-energy state of reduced spin multiplicity, as a result of the increase in inter-electron repulsion [4]. A second applies particularly to those lanthanides (e.g., Sm III, Eu III, Tm III and Yb III) that have low-energy ligand-to-metal-f charge-transfer (CT) states [7]. Configuration interactions between these CT states and the $f^N$ manifold provides a description of f-orbital covalency that can incorporate a degree of spin-polarization [6]. Tm III ought to provide the simplest and most clear-cut demonstration of the latter effect, because the influence of spin on the wavefunction expansion is calculated to be small for the heaviest lanthanides [8], while CT transitions occur at particularly low energies [9].

There are a number of reports of absorption and luminescence spectroscopy of Tm III in a chloride lattice [10–12], as well as CF parametrizations for cubic Tm III [12–14]. In 1985 it was suggested [12, 15] that a one-electron CF parametrization of Tm III was inadequate. This argument was based on small deviations from the one-body model in a number of low-lying energy levels, and its conclusions were vulnerable to the possible mis-assignment of some of those levels. Indeed it was pointed out later [16] that these observations were insufficient for an extended parametrization, and that data were specifically required for the $^1I_6$, $^1D_2$, $^3P_{2,1,0}$ multiplet manifolds before such a scheme could be meaningfully applied. In this work we have obtained these data, and are able to demonstrate that, for Tm III in a chloride ion environment, deviations from the one-electron CF theory are indeed unusually large.

## 2. Experiment

$Cs_2NaYCl_6$:Tm crystals were grown from the fused component binary chlorides by the Bridgman method. NaCl (99.999%) and CsCl (99.9%) were purified by vacuum sublimation. Anhydrous $TmCl_3$ and $YCl_3$ were prepared from $Ln_2O_3$ by vacuum decomposition of $(NH_4)_3[LnCl_6]$. Any oxychloride present was converted to chloride by exposing the freshly made $TmCl_3$ to a stream of dry HCl gas at 700 °C for 5 days (450 °C, 36 h for $YCl_3$). NaCl, CsCl and $LnCl_3$ powders in the appropriate ratio were mixed and transferred into an HF etched

Bridgman tube. $Cs_2NaYCl_6$:Tm was prepared by growth at a temperature of 750–800 °C under $Cl_2$ which was introduced to prevent the formation of divalent rare earths.

For ease of reference, we show in figure 1 a diagram of the free-ion states of Tm III. The parameters used to obtain these energies are those obtained for $Cs_2NaY_{0.95}Tm_{0.05}Cl_6$ in this work, as detailed in the results section. Two-photon excitation spectra require the choice of a suitable emission wavelength for detection. Thulium III emission from $^1D_2$ is documented [17], and our two-photon excitation spectra for $^1D_2$ (figure 3, below) are detected by means of the $^3F_4 \leftarrow {}^1D_2$ emission, using an interference filter of width 10 nm, centred at 450 nm.

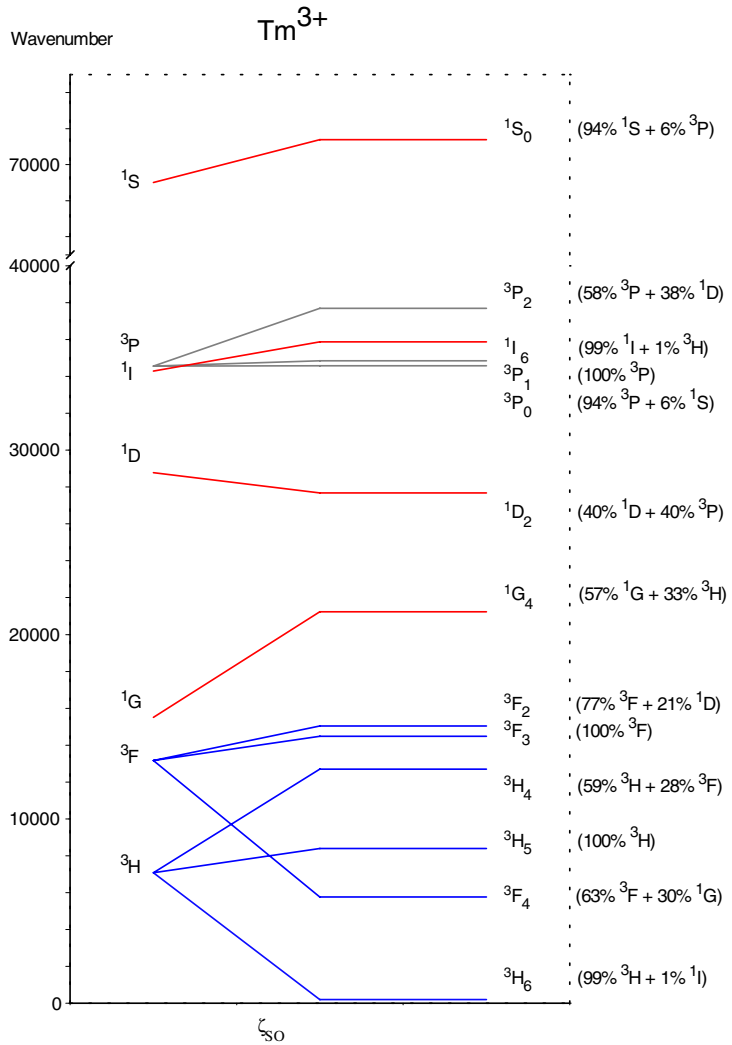


**Figure 1.** Energy level diagram for thulium III in zero field, illustrating the effects of spin–orbit coupling. The levels were calculated using the free-ion parameters for $Cs_2NaTm_{0.05}Y_{0.95}Cl_6$ in table 2. $|LS\rangle$ energies are determined by setting spin–orbit coupling to zero.

Figure 2 shows the 77 K fluorescence spectrum obtained under single-photon excitation at 285 nm (35 100 $cm^{-1}$) in the region of the $^1I_6$ absorption, which is the principal region of interest in this work. We assign the bulk of the emission to transitions from $^1I_6$ to $^3H_6$, $^3F_4$ and $^3H_5$.

For this reason, we chose broadband emission in the range 300–400 nm to probe the two-photon absorption (in figures 4 and 5, below). This region is far from the exciting wavelength (550–600 nm) and eliminates the detection of scattered laser light, but encompasses the resonance emission from $^1D_2$ (355 nm) should internal cross-relaxation processes depopulate $^1I_6$. The $^3F_4 \leftarrow {}^1I_6$ transition (at 345 nm) has also been successfully used as a two-photon probe in Tm:$LaF_3$ [18].

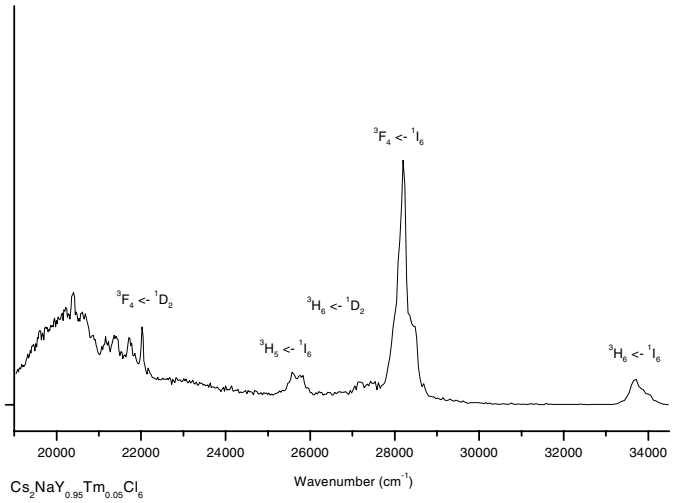


**Figure 2.** Fluorescence spectrum $Cs_2NaTm_{0.05}Y_{0.95}Cl_6$ at 77 K, excitation at 285 nm.

Experimental details for two-photon excitation spectroscopy have been reported previously [2]. Photons were counted for a period of 1 ms following a 100 $\mu$s delay after the laser pulse. The emission lifetimes at 350 and 450 nm for 5% Tm III doped crystals was $\sim$250 $\mu$s at 77 K.

## 3. Results

Figure 3 shows the TPE spectra in the region of $^1D_2$ where the two components, bands 28 ($T_{2g}$) and 29 ($E_g$), are easily assigned at 4 K. We find a CF splitting of 50 cm$^{-1}$. Although the crystal axes were not deliberately aligned relative to the beam direction, the incident polarization could be chosen to minimize the intensity in the lower-energy $T_{2g}$ band, which is strictly forbidden in the 0° polarization [1]. The polarization of this feature is not perfect, but compares with that achieved in cut crystals. More generally, the degree of polarization is sufficient to distinguish transitions designated as polarized in the 0 and 45° directions in our previous TPE studies [1–3], and can be used to identify the symmetry of the levels in figure 4, which we assign to the $^1I_6$ region. Hot-band features, and their temperature dependence, place the energies of the first two excited components of the $^3H_6$ multiplet at 56 and 148 cm$^{-1}$, confirming the assignment of [14] rather than [12].

The TPE spectrum in the region of $^1I_6$ (figure 4) is assigned as follows. Band 30 ($E_g$) is clearly polarized at 0°, as expected. Band 31 ($T_{2g}$) is weak at 4 K, but the hot-band structure confirms its position. The $^1I_6$ ($A_{2g}$) component 32 is strictly forbidden in TPE and is not located, although its presence is suggested by a hot-band structure at $\sim$34 400 cm$^{-1}$. Band 33 ($T_{2g}$) is strongly polarized at 45°. Band 34 is unpolarized ($A_{1g}$) and, because of its anomalous

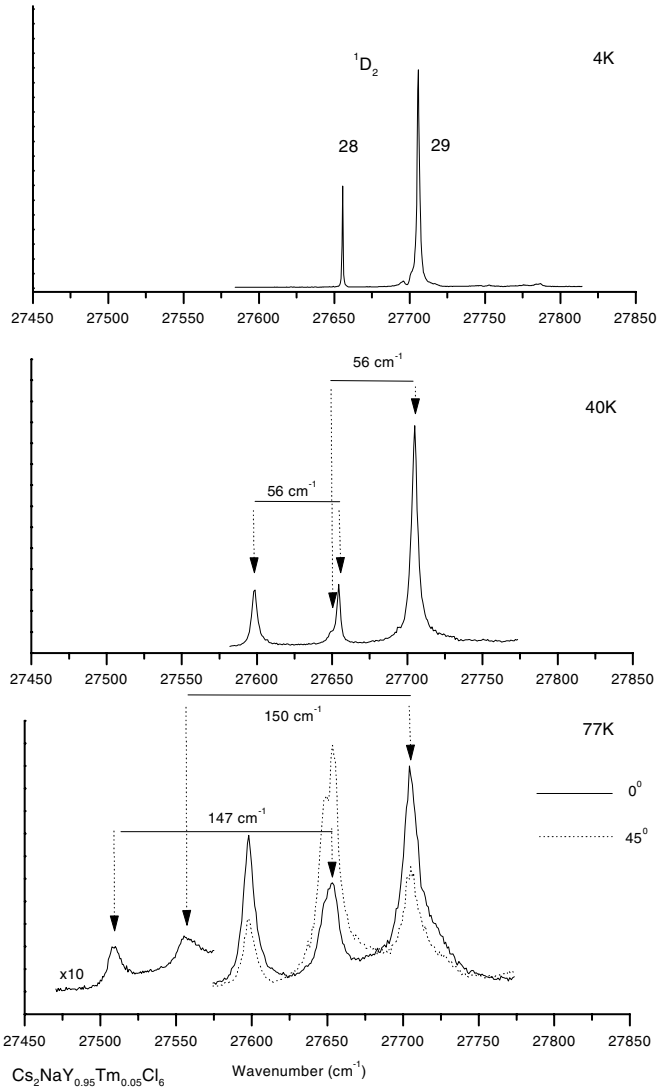


**Figure 3.** TPE spectra for $Cs_2NaTm_{0.05}Y_{0.95}Cl_6$ $^1D_2$. The numbers indicate the final state level sequence in table 1.

proximity to 33 when compared to that predicted by theory (see below), is assigned to the intruding $^3P_0$ origin. The associated 56 cm$^{-1}$ hot band ($A_{1g} \leftarrow T_{1g}$) is forbidden and is absent. Band 35 ($T_{1g}$) is forbidden from the electronic ground state, but the intense hot-band (56 cm$^{-1}$) at 34 920 cm$^{-1}$ is readily assigned to the allowed $T_{1g} \rightarrow T_{1g}$ transition. The broad unpolarized structure at 35 084 cm$^{-1}$ is the most credible assignment for 36 ($A_{1g}$), but is not included in the count of fitted levels (36 in total): its first hot-band is again forbidden, and the second hot-band (148 cm$^{-1}$) may overlap the hot-band structure at 34 920 cm$^{-1}$. The absorption near 35 800 cm$^{-1}$ is absent at 4 K, and we assign it to the $^3P_1$ 37 ($T_{1g}$) state, to which transitions are forbidden from the ground state. We are unable, however, to assign the features near 35 200 cm$^{-1}$.

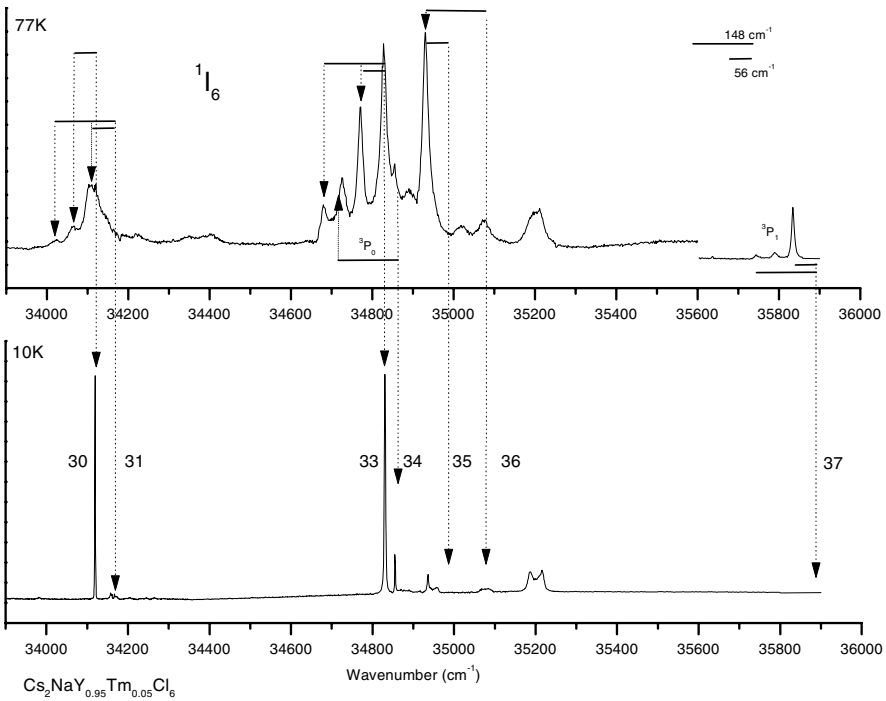


**Figure 4.** TPE spectra for $Cs_2NaTm_{0.05}Y_{0.95}Cl_6$ $^1I_6$, $^3P_{0,1}$. The numbers indicate the final state level sequence in table 1.

In lanthanide two-photon absorption [1–3] it is essential that there be a window at the laser wavelength free of one-photon absorption, in order to avoid resonant excited state absorption (sequential two-photon absorption or upconversion). In Tm III the sparseness of excited states makes the likelihood of one- and two-photon coincidence improbable. No up-conversion fluorescence was detected in the regions near 700 and 580 nm used for the excitation.

Figure 5 shows the TPE in the spectral region just below $^1I_6$ in energy. We are unable to assign the weak transitions labelled with a star. They are common to those observed in our earlier study of Tb III in $Cs_2NaTbCl_6$ [1], where it proved impossible to assign them to transitions of the Tb III ion. Since the fluorescence detection wavelength was very different in the Tb III case, we ascribe the additional transitions to two-photon absorption by a common but unknown lanthanide impurity, followed by energy transfer to Tm III or Tb III ions. We have studied the TPE spectra of Sm III, Eu III and Gd III in detail and can reject these ions as impurity candidates. The most likely common impurities are the intervening Ho III and Er III ions. The 10–15 cm$^{-1}$ red shift observed on going from 4 to 77 K is larger than we have usually observed for lanthanide two-photon lines, and may suggest the presence of Ho III, which has a crystal field component at $\sim$10 cm$^{-1}$ [14]. Resonantly enhanced transitions in Nd III [19] are also a possibility.

Table 1 records the levels determined experimentally in this work, along with literature results (italicized) from [11, 14] for $Cs_2NaTmCl_6$ and $Cs_2NaYCl_6$:Tm. Only very minor differences are recorded between the pure and 1% Tm doped systems [11], so these data sets are combined in the table. Table 2 shows the parameters derived from a SCCF fit to the experimental energy levels. Results obtained with a simple one-body Hamiltonian (table 3, column 2) were unsatisfactory, giving a standard deviation between the experimental and calculated energies twice as large as that obtained using a SCCF.

**Table 1.** Observed and calculated energy levels of Tm III in $Cs_2NaYCl_6$ (the levels in italics are taken from [11, 14]).

| Band | $\|LSJ\rangle$ | Symmetry | Energy ($cm^{-1}$) | Calculated $E$ ($cm^{-1}$) | $\Delta E$ |
|---|---|---|---|---|---|
| 1 | $^3H_6$ | $A_{1g}$ | 0 | 1 | −1 |
| 2 | $^3H_6$ | $T_{1g}$ | 56 | 57 | −1 |
| 3 | $^3H_6$ | $T_{2g}$ | 148 | 121 | 27 |
| 4 | $^3H_6$ | $A_{2g}$ | *261* | 239 | 22 |
| 5 | $^3H_6$ | $T_{2g}$ | *370* | 370 | 0 |
| 6 | $^3H_6$ | $E_g$ | *394* | 395 | −1 |
| 7 | $^3F_4$ | $T_{2g}$ | *5547* | 5515 | 32 |
| 8 | $^3F_4$ | $E_g$ | *5814* | 5839 | −25 |
| 9 | $^3F_4$ | $T_{1g}$ | *5866* | 5891 | −25 |
| 10 | $^3F_4$ | $A_{1g}$ | *5938* | 5959 | −21 |
| 11 | $^3H_5$ | $T_{1g}$ | *8241* | 8263 | −22 |
| 12 | $^3H_5$ | $E_g$ | *8270* | 8296 | −26 |
| 13 | $^3H_5$ | $T_{2g}$ | *8436* | 8440 | −4 |
| 14 | $^3H_5$ | $T_{1g}$ | *8532* | 8539 | −7 |
| 15 | $^3H_4$ | $T_{2g}$ | *12 538* | 12 540 | −2 |
| 16 | $^3H_4$ | $E_g$ | *12 607* | 12 653 | −46 |
| 17 | $^3H_4$ | $T_{1g}$ | *12 840* | 12 755 | 85 |
| 18 | $^3H_4$ | $A_{1g}$ | *12 882* | 12 899 | −17 |
| 19 | $^3F_3$ | $A_{2g}$ | — | 14 377 | — |
| 20 | $^3F_3$ | $T_{2g}$ | *14 431* | 14 437 | −6 |
| 21 | $^3F_3$ | $T_{1g}$ | *14 457* | 14 435 | 22 |
| 22 | $^3F_2$ | $E_g$ | *14 959* | 14 952 | 7 |
| 23 | $^3F_2$ | $T_{2g}$ | *15 133* | 15 136 | −3 |
| 24 | $^1G_4$ | $T_{2g}$ | *20 852* | 20 834 | 18 |
| 25 | $^1G_4$ | $E_g$ | *21 356* | 21 349 | 7 |
| 26 | $^1G_4$ | $T_{1g}$ | *21 424* | 21 427 | −3 |
| 27 | $^1G_4$ | $A_{1g}$ | *21 508* | 21 516 | −8 |
| 28 | $^1D_2$ | $T_{2g}$ | 27 656 | 27 644 | 12 |
| 29 | $^1D_2$ | $E_g$ | 27 706 | 27 708 | −2 |
| 30 | $^1I_6$ | $E_g$ | 34 120 | 34 131 | −11 |
| 31 | $^1I_6$ | $T_{2g}$ | 34 167 | 34 180 | −13 |
| 32 | $^1I_6$ | $A_{2g}$ | — | 34 352 | — |
| 33 | $^1I_6$ | $T_{2g}$ | 34 830 | 34 804 | 26 |
| 34 | $^3P_0$ | $A_{1g}$ | 34 855 | 34 855 | 0 |
| 35 | $^1I_6$ | $T_{1g}$ | 34 986 | 34 955 | 31 |
| 36 | $^1I_6$ | $A_{1g}$ | 35 084 | 35 087 | −3 |
| 37 | $^3P_1$ | $T_{1g}$ | 35 891 | 35 886 | 5 |
| 38 | $^3P_2$ | $E_g$ | *37 455* | 37 480 | −25 |
| 39 | $^3P_2$ | $T_{2g}$ | *37 848* | 37 837 | 11 |
| 40 | $^1S_0$ | $A_{1g}$ | — | 71 136 | — |

We have also calculated sets of parameters, derived from a one-body Hamiltonian, that fit those levels which have, on the one hand, more than 90% triplet parentage, and, on the other hand, more than 90% singlet parentage (table 3). For this purpose, the 'triplet' manifold is comprised of the free-ion levels designated by $^3H_6$, $^3H_5$ and $^3H_3$, and the 'singlet' manifold of those designated by $^1I_6$, $^1D_2$ and $^3P_2$. The inclusion of the state labelled $^3P_2$ amongst the singlets may appear surprising, until it is realized that the free-ion states bearing the notional

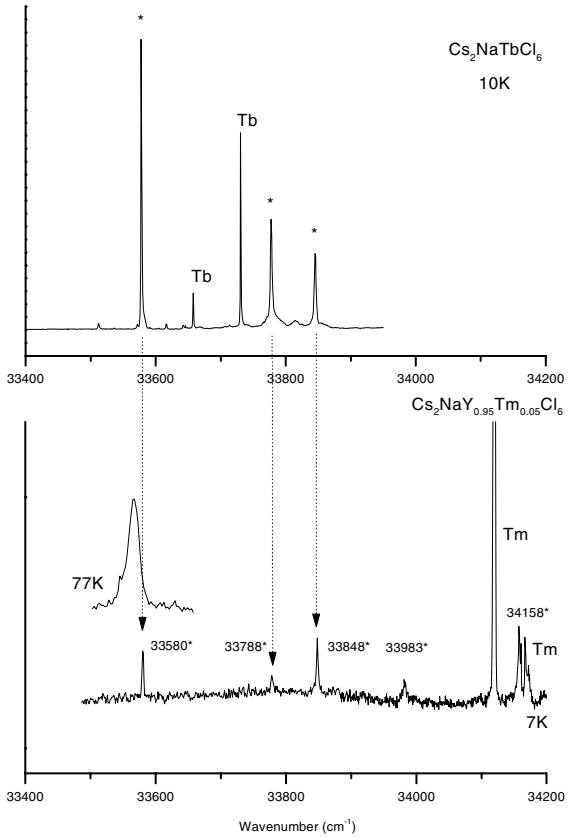


**Figure 5.** TPE spectra for $Cs_2NaTm_{0.05}Y_{0.95}Cl_6$ and $Cs_2NaTbCl_6$ illustrating the presence of a common impurity.

$^1D_2$, $^3P_2$ labels are both approximately equal superpositions of the $^3P$ and $^1D$ bases (figure 1), and that the $^3P$ basis is not split in the cubic CF. CF interactions in this set therefore originate only from singlet basis states. $^3P_1$ and $^3P_0$ are both unperturbed by the CF in first order, and were included in both subsets. In these optimizations only the CF parameters were varied, the remainder being held at the values obtained in the SCCF optimization.

This procedure provides *effective* one-body CF parameters applicable within each subset. The CF parameters for the 'triplet' subset (column 3) are similar to those obtained in earlier studies [10–12]. However, the effective CF applicable to the 'singlet' states (column 4) is ∼60% greater than that for the 'triplets'. The one-body fit to the complete set of states (column 2), yields CF parameters that are an approximate average of those applicable in the separate subsets. The inability of a single pair of CF parameters to describe both subsets is clearly the reason for the large standard deviation in this case.

## 4. Discussion

### *4.1. Deviations from the one-body CF model*

Automated parameter optimizations, such as those described above, inevitably add complexity to the interpretation of the dependence of the CF on the spin multiplicity. In this section,

**Table 2.** Energy parameters for $Cs_2NaYCl_6$:Tm, $M^2 = 0.560M^0$, $M^4 = 0.310M^0$; $P^4 = 0.750P^2$, $P^6 = 0.10P^2$.

| Parameter | $Cs_2NaYCl_6$:Tm |
|---|---|
| $E_{av}$ | 17 783.5 |
| $F^2$ | 99 444 |
| $F^4$ | 68 104 |
| $F^6$ | 47 788 |
| $\alpha$ | 17.5 |
| $\beta$ | −697 |
| $\gamma$ | 2888 |
| $\zeta_{so}$ | 2614 |
| $M^0$ | 3.8 |
| $P^2$ | −22 |
| $B_0^{(4)}$ | 2376 |
| $B_0^{(6)}$ | 255 |
| $b_0^{(4)}$ | 976 |
| $b_0^{(6)}$ | 61 |
| $c_0^{(4)}$ | $+0.41 \pm 0.05$ |
| $c_0^{(6)}$ | $+0.24 \pm 0.05$ |
| $\sigma$ | 28.2 |
| $N$ | 36 |

**Table 3.** One-body CF parameters for $Cs_2NaYCl_6$:Tm.

| Level | All | 'Triplets' | 'Singlets' |
|---|---|---|---|
| Free parameters | 12 | 3 | 3 |
| Number of levels | 36 | 14 | 10 |
| $\sigma$ | 55 | 36 | 22 |
| $B_0^{(4)}$ | 1919 | 1483 | 2396 |
| $B_0^{(6)}$ | 214 | 189 | 250 |

therefore, we seek to clarify this dependence by closer examination of the $^3H_6$, $^3H_5$ and $^1I_6$ multiplets. As a first step, the splitting of these multiplets will be shown to be well described by first-order interactions. Since $^3H_5$ is the only multiplet with $J = 5$, its composition in the free-ion $|LSJ\rangle$ basis is unique. Similarly, although some admixture of the $^3H_6$ and $^1I_6$ bases is to be expected, the eigenvectors of the free-ion Hamiltonian indicate that the $|LSJ\rangle$ purity of these states is greater than 99.1%. In other words, the Russell–Saunders approximation accurately describes all three multiplets.

Of course, the CF can mix states of different $J$. However, a Hamiltonian that fits the CF components of the triplet states satisfactorily, yields eigenvectors indicating that $J$-mixing is insignificant in almost all cases. For example, the probability contribution associated with the dominant $|^3H_6, M_J\rangle$ basis states in the six CF components of $^3H_6$, is always greater than 99.7%. For the components of $^3H_5$ and $^1I_6$, the corresponding figures are 99.3% and 99.6% respectively. There is, however, a single exception. The $A_{1g}$ component of $^1I_6$ is predicted (on the basis of the parameters used in this calculation) to be substantially intermingled with the $A_{1g}$ state arising from $^3P_0$, with which it is nearly degenerate—their separation being $\sim 60\,cm^{-1}$. However, it is apparent from the discussion in the previous section that the effective CF applicable to the $^1I_6$ multiplet should be very substantially larger. When this correction is applied, the compositional purity of $^1I_6(A_{1g})$ is close to 98%.

A first-order description of the CF splitting of all three multiplets should therefore give a good description of the energies. This is confirmed in table 4 by comparing these energies, obtained by standard tensor methods [20], with those derived using the full Hamiltonian matrix. In both calculations, the $B_0^{(4)}$ and $B_0^{(6)}$ parameters are those that provide the best fit to the triplet manifold (table 3). In all three multiplets it is clear that the errors attributable to the first-order approximation are small. In the first-order calculations, the centre of gravity of each set of the calculated levels was set equal to that of the experimental levels.

**Table 4.** First-order energy level calculation for $Cs_2NaYCl_6$:Tm (using 'triplet' CF parameters from table 3: $\sigma_E$ is defined in equation (4)).

| Parameter | Observed ($cm^{-1}$) | First order ($cm^{-1}$) | Full matrix ($cm^{-1}$) |
|---|---|---|---|
| $^3H_6$ | | | |
| $A_{1g}$ | 0 | 9 | 0 |
| $T_{1g}$ | 56 | 60 | 59 |
| $aT_{2g}$ | 148 | 123 | 127 |
| $A_{2g}$ | 261 | 255 | 260 |
| $bT_{2g}$ | 370 | 392 | 392 |
| $E_g$ | 394 | 420 | 418 |
| $\sigma_E$ | 145.2 | 156.8 | 157.1 |
| $^3H_5$ | | | |
| $aT_{1g}$ | 8263 | 8253 | 8271 |
| $E_g$ | 8296 | 8294 | 8306 |
| $T_{2g}$ | 8440 | 8443 | 8461 |
| $bT_{1g}$ | 8539 | 8547 | 8563 |
| $\sigma_E$ | 112.8 | 119.2 | 119.8 |
| $^1I_6$ | | | |
| $E_g$ | 34 120 | 34 316 | 34 318 |
| $bT_{2g}$ | 34 167 | 34 351 | 34 351 |
| $A_{2g}$ | 34 352 | 34 467 | 34 464 |
| $aT_{2g}$ | 34 830 | 34 745 | 34 740 |
| $T_{1g}$ | 34 986 | 34 832 | 34 831 |
| $A_{1g}$ | 35 084 | 34 906 | 34 921 |
| $\sigma_E$ | 384.5 | 229.2 | 229.6 |

A convenient measure of the effective CF within a multiplet is the splitting parameter $\sigma_E$, defined as the square root of the second moment of the energies of the components, i.e.

$$\sigma_E^2([\alpha SL]J) = \frac{1}{2J+1}\sum_n \{E_n - \bar{E}([\alpha SL]J)\}^2 \tag{4}$$

where $\bar{E}$ is the mean energy of the $2J + 1$ components. We have previously used the $\sigma_E$ parameter to test for deviations between experimental splittings and those predicted by the one-body CF Hamiltonian in a large number of multiplets of the Tb III ion [1]. Leavitt [21] has shown that in the Russell–Saunders limit and in the absence of $J$-mixing, the second moment is given by

$$\sigma_E^2([\alpha SL]J) = \frac{1}{2J+1}\sum_k s_k^2 \langle [\alpha SL]J \| C^{(k)} \| [\alpha SL]J \rangle^2 \tag{5}$$

where $s_k$ is a $k$th-rank field-strength parameter, defined by the rotationally invariant expression

$$s_k = \left( \frac{1}{2k+1} \sum_q |B_{kq}|^2 \right)^{1/2} \tag{6}$$

in which the $B_{kq}$ are the Wybourne CF parameters. In equation (5) the reduced matrix elements are those of the spherical tensor operators, $\hat{C}_q^{(k)}$. In this paper we report the CF parameters $B_q^{(k)}$ that multiply the matrix elements of the unit tensor operators $\hat{U}_q^{(k)}$. For f-electron states, the alternate definitions are such that $B_q^{(k)} = B_{kq}\langle 3\|C^{(k)}\|3\rangle$, so that $B_{40} = \sqrt{11/14}B_0^{(4)}$ and $B_{60} = -\sqrt{429/700}B_0^{(4)}$. Given the compositional purity of $^3H_6$, $^3H_5$ and $^1I_6$, a meaningful value of the splitting parameter, $\sigma_E$, for each multiplet can be obtained using equation (5). Table 5 contains the necessary reduced matrix elements for this purpose.

**Table 5.** Reduced matrix elements of the $\hat{C}^{(k)}$ operators.

| $\|LSJ\rangle$ | $\langle J\|C^{(4)}\|J\rangle$ | $\langle J\|C^{(6)}\|J\rangle$ |
|---|---|---|
| $^3H_6$ | $-\frac{8}{99}\sqrt{\frac{1547}{11}}$ | $+\frac{25}{33}\sqrt{\frac{323}{143}}$ |
| $^3H_5$ | $-\frac{8}{9}\sqrt{\frac{13}{22}}$ | $+\frac{1}{3}\sqrt{\frac{255}{143}}$ |
| $^1I_6$ | $+\frac{4}{33}\sqrt{\frac{1547}{11}}$ | $-\frac{10}{33}\sqrt{\frac{323}{143}}$ |

Values of the splitting parameter, $\sigma_E$, calculated in this way are included in column 2 of table 4. We have confirmed that they are identical to those obtained from the square root of the second moment of the first-order energies of the individual components, when these are calculated explicitly. Table 4 shows that these $\sigma_E$ values are almost indistinguishable from those calculated using the full Hamiltonian matrix in which the CF is represented by a one-electron operator (column 3).

It follows that the $\sigma_E$ value is a useful indicator of the effective CF within these multiplets. We note in particular that the ratio of the absolute value of the *calculated* splittings, $\sigma_E(^1I_6)/\sigma_E(^3H_6)$ is 1.46. Given that the fourth-rank terms in the potential dominate the splitting, this factor is close to that (i.e. $-3/2$) expected from the reduced matrix elements of $\hat{C}_q^{(4)}$ (table 5). The reduced matrix elements of $\hat{C}_q^{(6)}$ are smaller by a factor of $-2/5$ in $^1I_6$ compared to $^3H_6$ (table 5). Consequently, the sixth-rank terms account for 2.8% of $\sigma_E$ in the $^3H_6$ multiplet, but only 0.4% in $^1I_6$.

Table 4 shows that the choice of $B_0^{(k)}$ parameters used for these calculations leads to a small negative deviation, as assessed by the quantity $(\sigma_{exp} - \sigma_{calc})/\sigma_{calc}$, of ~7% between the experimental and calculated values of $\sigma_E$ in the $^3H_6$ and $^3H_5$ multiplets. This small difference reflects the use of CF parameters optimized to all the states in the 'triplet' subset, rather than those in these multiplets alone. By contrast the experimental value of $\sigma_E = 384.5$ cm$^{-1}$ in the $^1I_6$ multiplet represents a deviation of +68%, when compared to that expected from the theoretical model. This is the main result of this work. (The $A_{2g}$ component of $^1I_6$ is not observed, so $\sigma_{E(exp)}$ is calculated using the energy predicted by the SCCF optimization instead. The error implied by this assumption should not be large, because the $A_{2g}$ state is relatively close to the mean energy of the manifold (figure 6), and it is only one of 13 levels whose energies define the splitting parameter.) The splitting parameter $\sigma_E$ for $^1I_6$ can alternatively be estimated from the experimental value for $^3H_6$ (145.2 cm$^{-1}$), rather than the theoretical value. If the later scaled is by the factor of 1.46 predicted by the calculation, $\sigma_E$ for $^1I_6$ should be 212 cm$^{-1}$. The increase of the experimental value (to 384.5 cm$^{-1}$) in relation to this prediction is +81%.

This large expansion of the $^1I_6$ manifold, relative to that expected from fitting the triplet data is illustrated in figure 6. In this diagram, column (a) represents the experimental levels, columns (b) and (c) show, respectively, a first-order and full matrix calculations with $B_0^{(4)} = -1483\,\mathrm{cm}^{-1}$ and $B_0^{(6)} = 189\,\mathrm{cm}^{-1}$. In column (d) the first-order energies of column (b) have been scaled by the factor 1.676 relative to the mean energy, and column (e) shows the results of a full SCCF calculation. It is clear that the experimental levels are rather well reproduced (in column (d)) by a simple linear expansion of the first-order multiplet splitting of $^1I_6$. This distinction is incorporated in the SCCF Hamiltonian, which effectively applies different radial parameters to the singlet and triplet manifolds.

### *4.2. SCCF coefficients and effective one-body CFs*

For the two-particle $f^2$ and $f^{12}$ ions, equation (3) implies that the CF Hamiltonian for the singlet states is equal to $H_{CF}$, but that for the higher multiplicity states contains an additional contribution $H_{SCCF}$. In terms of effective CF parameters, we obtain from Judd [5]:

$$B_0^{(k)}{}_{effective}(S=0)/B_0^{(k)}{}_{effective}(S=S_{MAX}) = 1/(1 \pm c_0^{(k)}(1+S_{MAX})/2) \tag{7}$$

in particular, for the two-particle $f^2$ and $f^{12}$ ions:

$$B_0^{(k)}{}_{effective}(S=0)/B_0^{(k)}{}_{effective}(S=1) = 1/(1 \pm c_0^{(k)}) \tag{8}$$

where the positive sign applies to $f^2$ and the negative sign to $f^{12}$. This equation, relating SCCF coefficients to effective one-body CFs, is exact for these two rare earth configurations. Clearly *positive* SCCF coefficients $c_0^{(k)}$ in equation (8) predict an increased effective CF in the singlet states of Tm III.

Experimentally, we observe (table 3) that the ratio of effective $B_0^{(4)}$ and $B_0^{(6)}$ of the 'singlet' ($S = S_{max} - 1 = 0$) and 'triplet' ($S = S_{max} = 1$) manifolds in the thulium chloro-elpasolite are 1.6 and 1.3, respectively. From equation (8) we indeed estimate positive SCCF parameters, $c_0^{(4)} = +0.38$ and $c_0^{(6)} = +0.24$, in excellent agreement with those obtained in the SCCF fit (table 2) ($c_0^{(4)} = +0.41$ and $c_0^{(6)} = +0.24$). These values of the SCCF parameters are some of the largest ever reported, values of $|c_0^{(k)}| \sim 0.1$ being more common for the lanthanides [4].

To estimate the ratio of effective $B_q^{(k)}$ parameters in neighbouring spin states, for configurations other than $f^2$ and $f^{12}$, we make an approximate equi-partition of the total change between the maximum and minimum spin states, given by equation (7), and divide it by the number of spin flips, $S_{MAX}$. Then,

$$B_0^{(k)}{}_{effective}(S=S_{MAX}-1)/B_0^{(k)}{}_{effective}(S=S_{MAX}) \cong 1/(1 \pm c_0^{(k)}(1+S_{MAX})/2S_{MAX}) \tag{9}$$

where the positive and negative signs apply to the first and second halves of the series respectively.

### *4.3. 'SCCF' mechanisms*

We now distinguish and discuss three distinct consequences of many-body interactions that can be manifest in a SCCF Hamiltonian. Their effect upon the effective CF parameters are summarized schematically in figure 7, together with our experimental data for $Cs_2NaLnCl_6$ (Ln = Sm, Eu, Tb, Tm). Curves (a) and (b) are based upon equation (9).

*4.3.1. Spin-correlated differential radial expansion: mechanism (a).* The expectation of the SCCF theory in its original form [5] is that the coefficients, $c_0^{(k)}$, ought to be *negative*. As such they were intended to express the notion that, in a spin-unrestricted self-consistent field basis,

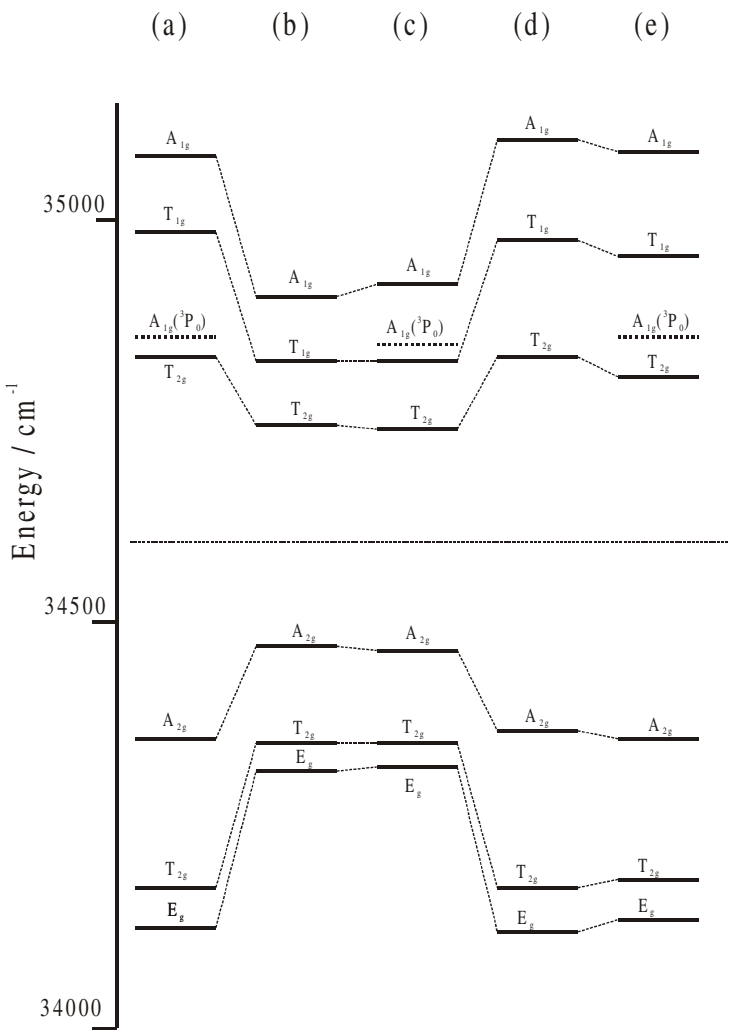


**Figure 6.** CF expansion in the $^1I_6$ manifold.

majority-spin electrons should have more contracted orbital radii than minority-spin electrons. The latter ought therefore to experience larger CF interactions. In the first half of the lanthanide series, states with $S < S_{max}$, in which the preponderance of majority-spin electrons is reduced relative to those with $S = S_{max}$, should show an increased splitting. On the other hand, in the second half of the series, the CF interactions of majority-spin electrons in states with $S = S_{max}$ sum to zero, and the CF energies are determined only by minority-spin electrons. In this case, the CF energies in states with $S < S_{max}$ have contributions from electrons of both spin orientations, and should show reduced splitting compared to those with $S = S_{max}$. This is shown in figure 7 curve a for an estimated parameter value $c_0^{(4)} = -0.1$ suggested by Judd [5].

The SCCF interaction is defined mathematically in terms of a two-body operator, whereas the CF is represented by one-body operators that change sign on going from $f^N$ to $f^{14-N}$. Thus the 'SCCF' perturbation, whatever its underlying physical basis, has an opposite effect on the absolute magnitude of the CF in the first and second halves of the series, leading to a

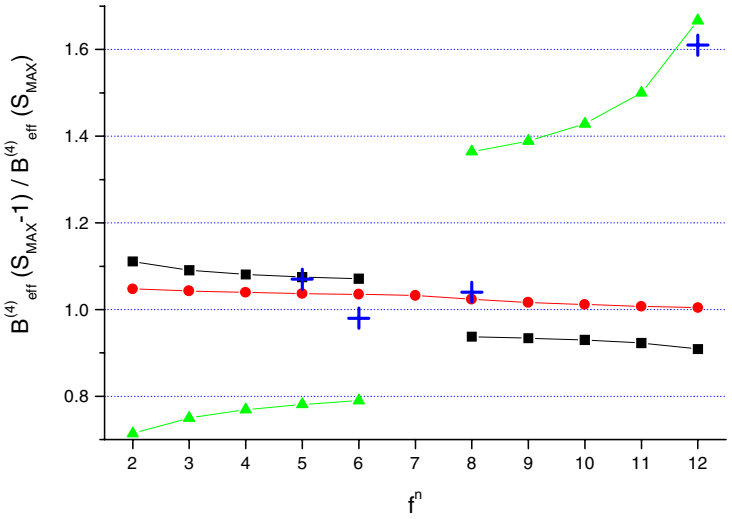


**Figure 7.** Dependence of effective CF for $f^N$: (a) spin-correlated differential radial expansion ($c = -0.1$) ■; (b) spin-polarized CT ($c = +0.4$) ▲; (c) radial expansion in low spin states ●; and (d) experimental data for $Cs_2NaLnCl_6$ (Ln = Sm, Eu, Tb, Tm) +.

discontinuity at the halfway point [6]. Indeed such a trend is observed, but its direction is not accounted for by the simple effects of spin-correlation as introduced above.

*4.3.2. Spin-polarized CT: mechanism (b).* Admission of ligand-to-metal CT, and the covalency implied thereby, provides an alternative mechanism that can be treated within the same parametrization scheme [6]. It predicts *positive* SCCF coefficients. The effect of covalency is described by means of an interaction, comprising both one- and two-electron operators, that links the $f^N$ states with those from CT configurations of the form $f^{N+1}\psi_L^{-1}$, where $\psi_L$ represents the set of filled ligand orbitals. Depending on the spin of the transferred electron, the CT states can be described by basis functions of the form $|f^{N+1}(S_{max} \pm \frac{1}{2})\psi_L(s = \frac{1}{2})\rangle$, where $S_{max}$ refers to the $f^N$ ground state. We now make the reasonable assumption that one-centre f-electron exchange interactions are much larger than two-centre exchange integrals that involve the ligand spin. The inter-f-electron exchange interactions therefore dominate the relative energies of the CT states. In the first half of the series, those CT states with total spin $S_{max}$, obtained by coupling the ligand spin to the $f^{N+1}(S_{max} + \frac{1}{2})$ configuration, therefore occur at lower energies than those with total spin $S_{max} - 1$ derived from the $f^{N+1}(S_{max} - \frac{1}{2})$ configuration.

This magnitude of this covalency exhibits a spin-polarization, and is larger for those $f^N$ states with $S = S_{max}$, relative to those with $S = S_{max} - 1$. The connection between covalency and the magnitude of the CF splitting is straightforward. Those f-orbitals that have covalent interactions with ligand orbitals are anti-bonding, and have their energy is raised compared to non-bonding orbitals. In the present description this is because their occupation blocks energy-lowering CT interactions. Increased CF parameters should therefore be expected in the $S_{max}$ manifold. Note that this outcome is exactly the opposite of that based on the consequences of single-centre spin-correlation (i.e. mechanism (a)). Figure 7 curve b plots an estimate of the effective ratio for $c_0^{(4)} = +0.4$ (the value we observe for Tm III).

The effects of CT should be at a maximum for Eu III, $f^6$, where the difference in exchange energy of the charge transfer configurations is large; being comparable to the separation of the

octet and sextet manifolds of Gd III, i.e. about 5.7 eV. More importantly, the relatively positive reduction potential of Eu III (−0.43 V) compared to other lanthanide III ions, indicates that the energies of the CT states, relative to the $f^N$ ground state, are low (∼4.0 eV [9]), so that this class of configuration interaction should be significant.

Electron transfer to the Tb III $f^8$ ion generates CT states that also differ markedly in their exchange energy, but the outcome is the opposite of that for Eu III. Thus the $S = 3$ (septet) ground state interacts with CT states in which the additional f-electron must be parallel to the (single) minority spin. However the $S = 2$ states mix with CT states in which the additional f-electron can be parallel to the (five) majority-spin electrons. In the second half of the series, then, the CT mechanism predicts increased covalency and larger CF interactions in states with $S < S_{max}$. (Note however that the low third ionization energy of Tb suggests that ligand-to-metal CT should not be significant in the Tb III ion.)

*4.3.3. Radial expansion in low-spin states: mechanism (c).* From an analysis of the available experimental data, we have found [4] that SCCF coefficients are clearly positive only in the second half of the series, but are often determined to be negative in the first half of the series. In particular an SCCF analysis for Pr III $f^2$ [22] produces values that are small and negative. We have argued [4] that this is indicative of a modification of the CF that is best accounted for by a radial expansion of all f-electron wavefunctions, regardless of their spin, in those states with $S < S_{max}$. The extent of this expansion can be estimated from the results of spin-restricted relativistic self-consistent field (SCF) calculations [4]. It is found to be of the correct magnitude [8] to account for the changes in $B_q^{(k)}$. This contribution is plotted as figure 7 curve c. In the absence of any strong differential admixture of CT into the ground and excited states, this feature would predict negative SCCF coefficients in the first half of the series and positive coefficients in the second half.

Of the three mechanisms (a), (b) and (c), we note that (b) and (c) make contributions of the same sign in the second half of the series, but opposite sign in the first half. This we believe to be the reason that positive SCCF coefficients are clearly established in the latter half of the series, while the signs are more equivocal in the first half.

### *4.4. CT states*

CT states are observed in the spectra of the trivalent ions of Ce, Sm, Eu, Tm and Yb in chloride and bromide lattices [7]. Of these, Ce and Yb are of no interest, because they possess only doublet f-electron states. We have discussed deviations from one-body CF theory for both Sm III [2] and Eu III [1], obtaining the values $c_0^{(4)} = -0.14$, $c_0^{(6)} = -0.3$ and $c_0^{(4)} = +0.04$, $c_0^{(6)} = +0.3$ respectively. CT states occur at particularly low energies for Eu III [9] so we attribute the small magnitude of these coefficients, and their change in sign to the near cancellation of mechanisms (b) and (c), with (c) becoming dominant in the Eu III case.

Thulium III is more straightforward. The relative radial expansion of the singlet states of the $f^{12}$ ion (i.e. mechanism (c)) is predicted to be small [8]. CT transitions have been observed in the $TmBr_6^{3-}$ lattice at a wavelength of ∼260 nm [7], and a comparison with other lanthanide hexa-halide complexes predicts analogous transitions in $TmCl_6^{3-}$ near 210 nm (48 000 $cm^{-1}$) [9]. The transfer of an electron, of either spin, generates CT states derived from the same $f^{13}$ doublet configuration of the thalium II ion. However CT states at 48 000 $cm^{-1}$ generated in this way, should mix much more effectively with the singlet states of Tm III near 35 000 $cm^{-1}$, than with the energetically distant triplets. We believe that the much increased CF in the singlet states of Tm III in a chloride environment, as expressed in large positive SCCF coefficients (table 2), is therefore dominated by the influence of differential CT mixing and covalency.

A preliminary TPE investigation of CF levels in $TmF_6^{3-}$, where the CT states lie at much higher energy, suggests that deviations from the one-body theory are much smaller in this lattice as would be expected for a CT mechanism. A more comprehensive study of a thulium III fluoro-elpasolite is required to quantify this point. However sufficient experimental data are available for Tm III in $LiYF_4$ [23] for the SCCF parameters to be estimated. Most of the components of the $^1D_2$ and $^1G_4$ have been identified together with two components of $^1I_6$, so the data set is less complete than that analysed in this work. The low site ($\sim D_{2d}$) symmetry requires additional CF parameters compared to the cubic case, and the SCCF analysis [24] yields the following values: $c_0^2 = 0.15$, $c_0^4 = 0.14$, $c_0^6 = 0.04$ and $c_4^6 = -0.24$. Those coefficients that can be compared with the cubic case are much smaller than those (section 4.2) in the chloride environment, and thus support the CT hypothesis.

## 5. Conclusions

Deviations from one-body CF theory have been shown to be very large ($\sim$65%) for Tm III in $Cs_2NaYCl_6$:Tm. This result is underpinned by two-photon selection rules and polarizations that provide a secure assignment of the majority of the CF components of the characteristic $^1I_6$ multiplet. These deviations are well described by the use of SCCF parameters.

We note that the SCCF is manifest most strongly in the *fourth-rank* CF parameters, which are of overwhelming importance in this instance. It is often argued that the *sixth-rank* SCCF parameters are of most significance, see for example [24] and references therein, but that is clearly not the case here. We believe the clear failure of the one-body model in the Tm III ion is a consequence of the preferential admixture of low-lying ligand-to-metal CT states into the singlet states of the ion, leading to a large increase in the effective one-body CF parameters, relative to those in the triplet states.

## Acknowledgments

We thank the Royal Society for support for QZ under the Royal Fellowships Programme, and the EPSRC Laser Support Facility, Rutherford Appleton Laboratory for the loan of a dye laser. We also thank M F Reid for allowing us to use his F-Shell program, and Dr Barbara Nissen for providing samples of the fluoride elpasolite $Rb_2NaYF_6$:Tm.

## References

[1] Morrison I D, Berry A J and Denning R G 1999 *Mol. Phys.* **96** 43
[2] Thorne J R G, Jones M, McCaw C S, Murdoch K M, Denning R G and Khaidukhov N M 1999 *J. Phys.: Condens. Matter* **11** 7851
[3] Thorne J R G, Karunathilake A, Han Choi, Denning R G and Luxbacher T 1999 *J. Phys.: Condens. Matter* **11** 7867
[4] Thorne J R G, McCaw C S and Denning R G 2000 *Chem. Phys. Lett.* **319** 185
[5] Judd B R 1977 *Phys. Rev. Lett.* **39** 242
[6] Newman D J, Siu G G and Fung W Y P 1982 *J. Phys. C: Solid State Phys.* **15** 3113
[7] Ryan J L and Jorgensen C K 1966 *J. Phys. Chem.* **70** 2845
[8] Vanquickenborne L G, Pierloot K and Gorller-Wallrand C 1986 *Inorg. Chim. Acta* **120** 209
[9] Ionova G, Krupa J C, Gerard I and Guillaumont R 1995 *New J. Chem.* **19** 677
[10] Schwartz R W, Faulkner T R and Richardson F S 1979 *Mol. Phys.* **38** 1767
[11] Foster D R, Reid M F and Richardson F S 1985 *J. Chem. Phys.* **83** 3225
[12] Tanner P A 1985 *Mol. Phys.* **54** 883
[13] Reid M F and Richardson F S 1985 *J. Chem. Phys.* **83** 3831
[14] Tanner P A, Ravi Kanth Kumar V V, Jayasankar C K and Reid M F 1994 *J. Alloys Compounds* **215** 349

[15] Tanner P A 1986 *J. Chem. Phys.* **85** 2344
[16] Richardson F S 1986 *J. Chem. Phys.* **85** 2345
[17] Kirk A D, Furer N and Guedel H U 1996 *J. Lumin.* **68** 77
[18] He-Yi Zhang, Xuehua He, Sing Hai Tang and Xiang-Xin Bi 1990 *Chem. Phys. Lett.* **171** 119
[19] Foster D R, Richardson F S and Schwartz R W 1985 *J. Chem. Phys.* **82** 601
Foster D R, Richardson F S and Schwartz R W 1985 *J. Chem. Phys.* **120** 209
[20] Judd B 1963 *Operator Techniques in Atomic Spectroscopy* (New York: McGraw-Hill)
[21] Leavitt R P 1982 *J. Chem. Phys.* **77** 1661
[22] Reid M F, Richardson F S and Tanner P A 1987 *Mol. Phys.* **60** 881
[23] Jennsen H P, Linz A, Leavitt R P, Morrison C A and Wortman D E 1975 *Phys. Rev.* B **11** 92
[24] Jayasankar C K, Reid M F and Richardson M F 1989 *Phys. Status Solidi* b **155** 559